Partial anhysteretic remanent magnetization in magnetite 2. Reciprocity

Yongjae Yu, David J. Dunlop, and Özden Özdemir

Geophysics, Department of Physics, University of Toronto, Toronto, Ontario, Canada

Received 20 September 2001; revised 1 March 2002; accepted 6 March 2002; published 23 October 2002.

[1] One necessary condition for successful determination of relative paleomagnetic field intensity using anhysteretic remanent magnetization (ARM) methods is reciprocity: a partial ARM, produced by a steady field H applied over a narrow interval ($\widetilde{H}_2$, $\widetilde{H}_1$) of alternating field (AF), must demagnetize over the same interval ($\widetilde{H}_2$, $\widetilde{H}_1$). Experimentally, we find that partial ARMs of single-domain (SD) and pseudosingle-domain (PSD) grains demagnetize mainly between $\widetilde{H}_2$ and $\widetilde{H}_1$, whereas >50% of partial ARMs of large PSD and multidomain (MD) grains are erased below $\widetilde{H}_1$, giving a low-field tail in the coercivity distribution. Natural pumices, granites, and oceanic basalts violated reciprocity, but lake sediments, gabbros, andesite, and red scoria had relatively small low-coercivity tails and are better candidates for paleointensity work. Using total ARM to simulate natural remanence, we carried out pseudo-Thellier paleointensity determinations for coarse PSD and MD grains. ARM demagnetization outweighed partial ARM acquisition at the same AF step, resulting in convex-down curves of ARM remaining versus partial ARM gained (pseudo-Arai plot). Pseudo-Arai plots predicted from experimentally determined distributions of blocking and unblocking fields agreed well with measured pseudo-Thellier results, in particular explaining convex-down MD curves. *INDEX TERMS:* 1540 Geomagnetism and Paleomagnetism: Rock and mineral magnetism; 1518 Geomagnetism and Paleomagnetism: Magnetic fabrics and anisotropy; 1521 Geomagnetism and Paleomagnetism: Paleointensity; 1594 Geomagnetism and Paleomagnetism: Instruments and techniques; *KEYWORDS:* reciprocity, magnetite, ARM, pseudo-Thellier, AF demagnetization, additivity

Citation: Yu, Y., D. J. Dunlop, and Ö. Özdemir, Partial anhysteretic remanent magnetization in magnetite, 2, Reciprocity, *J. Geophys. Res.*, *107*(B10), 2245, doi:10.1029/2001JB001269, 2002.

1. Introduction

[2] Thellier's laws of additivity, reciprocity and independence of partial thermoremanent magnetization (pTRM) are valid for single-domain (SD) grains and form the basis of Thellier-type methods of paleointensity determination [*Thellier*, 1938; *Thellier and Thellier*, 1959]. The reciprocity law states that pTRM produced by applying a field H between T_2 and T_1 ($T_2 > T_1$) during cooling from the Curie temperature and zero field in all other temperature intervals is thermally demagnetized during zero-field heating over precisely the temperature interval (T_2, T_1). In other words, blocking temperature equals unblocking temperature. Any violation of the reciprocity law will result in failure of paleointensity determination.

[3] In paper 1 [*Yu et al.*, 2002], we test a law analogous to the Thellier additivity law, using partial anhysteretic remanent magnetization (pARM) instead of pTRM and alternating field (AF) demagnetization instead of thermal demagnetization. The present paper tests the analog of the Thellier reciprocity law: pARM produced by a steady field H applied only in the AF interval ($\widetilde{H}_2$, $\widetilde{H}_1$) must be AF demagnetized over precisely the interval ($\widetilde{H}_2$, $\widetilde{H}_1$). In other words, blocking field equals unblocking field.

0148-0227/02/2001JB001269$09.00

2. Samples and Experiments

[4] The 10 synthetic and 18 natural magnetite- or titanomagnetite-bearing samples described in Tables 1–3 of paper 1 were again used. Magnetic grains of particular coercivities were isolated as narrowband pARMs produced over narrow intervals of AF using a Molspin demagnetizer. The standard initial state was AF demagnetized in a peak AF of 100 mT. The sequence of steps in experiments testing the reciprocity of pARM was as follows (Figure 1).

1. First, $pARM^m$ ($\widetilde{H}_b$, $\widetilde{H}_a$) was produced by a steady field H applied over the AF interval from $\widetilde{H}_b$ to $\widetilde{H}_a$; from $\widetilde{H}_a$ to 0 mT, there was zero added field.

2. AF demagnetization was performed in either 2.5 or 5 mT steps. Double demagnetization [*Tauxe et al.*, 1995] was carried out along orthogonal axes (x, y, z), followed by ($-x$, $-y$, $-z$), with remanence being measured after each set of three demagnetizations and then vectorially averaged.

3. Next, $pARM^n$ ($\widetilde{H}_d$, $\widetilde{H}_c$) was produced as in step 1 but using a higher AF interval ($\widetilde{H}_d$, $\widetilde{H}_c$).

4. Double AF demagnetization of $pARM^n$ ($\widetilde{H}_d$, $\widetilde{H}_c$).

[5] The intervals ($\widetilde{H}_b$, $\widetilde{H}_a$) and ($\widetilde{H}_d$, $\widetilde{H}_c$) were determined from prior AF demagnetization of total ARM. They corre-

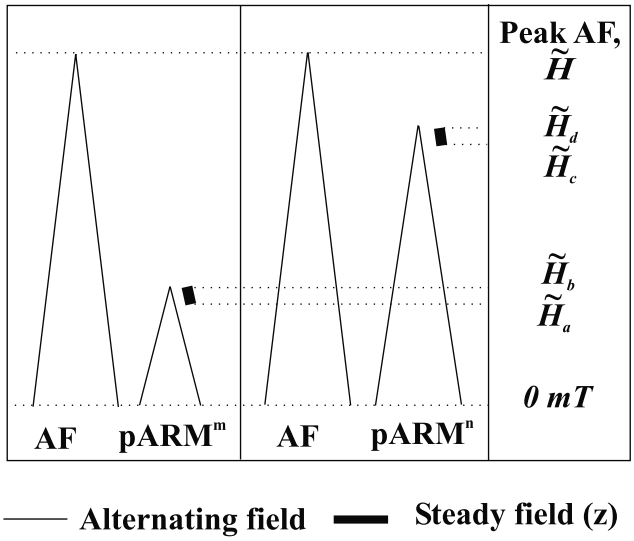

Figure 1. Schematic diagrams representing pARM acquisition: pARM^m ($\tilde{H}_b$, $\tilde{H}_a$) and pARM^n ($\tilde{H}_d$, $\tilde{H}_c$) were produced starting from peak AFs of $\tilde{H}_b$ and $\tilde{H}_d$ with the added steady field H on from $\tilde{H}_b$ to $\tilde{H}_a$ and from $\tilde{H}_d$ to $\tilde{H}_c$, respectively.

spond to 30–40% and 60–70% destruction of ARM. Thus pARM^m and pARM^n represent soft and hard coercivity fractions. Initial remanence in the AF demagnetized state, where significant, was vector subtracted from all pARMs. The steady field H of 50–100 μT was applied along the cylindrical (z) axis of the specimen.

3. Results

3.1. Synthetic Samples

[6] In AF demagnetization of samples 1–6, which contain SD or pseudosingle-domain (PSD) grains, the remanence dropped quite sharply over the pARM blocking range (dashed lines; Figures 2a and 2b), particularly for the lower coercivity pARM. Coercivity spectra $\Delta(M/M_0)/\Delta\tilde{H}$ (Figure 2c) show that >80% of pARM^m of SD sample 1 (0.065 μm) demagnetized over the AF blocking interval 20–25 mT. The results for pARM^n (50, 45 mT) are similar but more remanence unblocks below the lower blocking field of 45 mT (Figures 2b and 2d).

[7] The pARM of multidomain (MD) magnetite samples behaved quite differently (Figure 3). Although no remanence unblocking occurred above the upper blocking field (15 or 40 mT in Figures 3a and 3b), 65–80% of the pARM

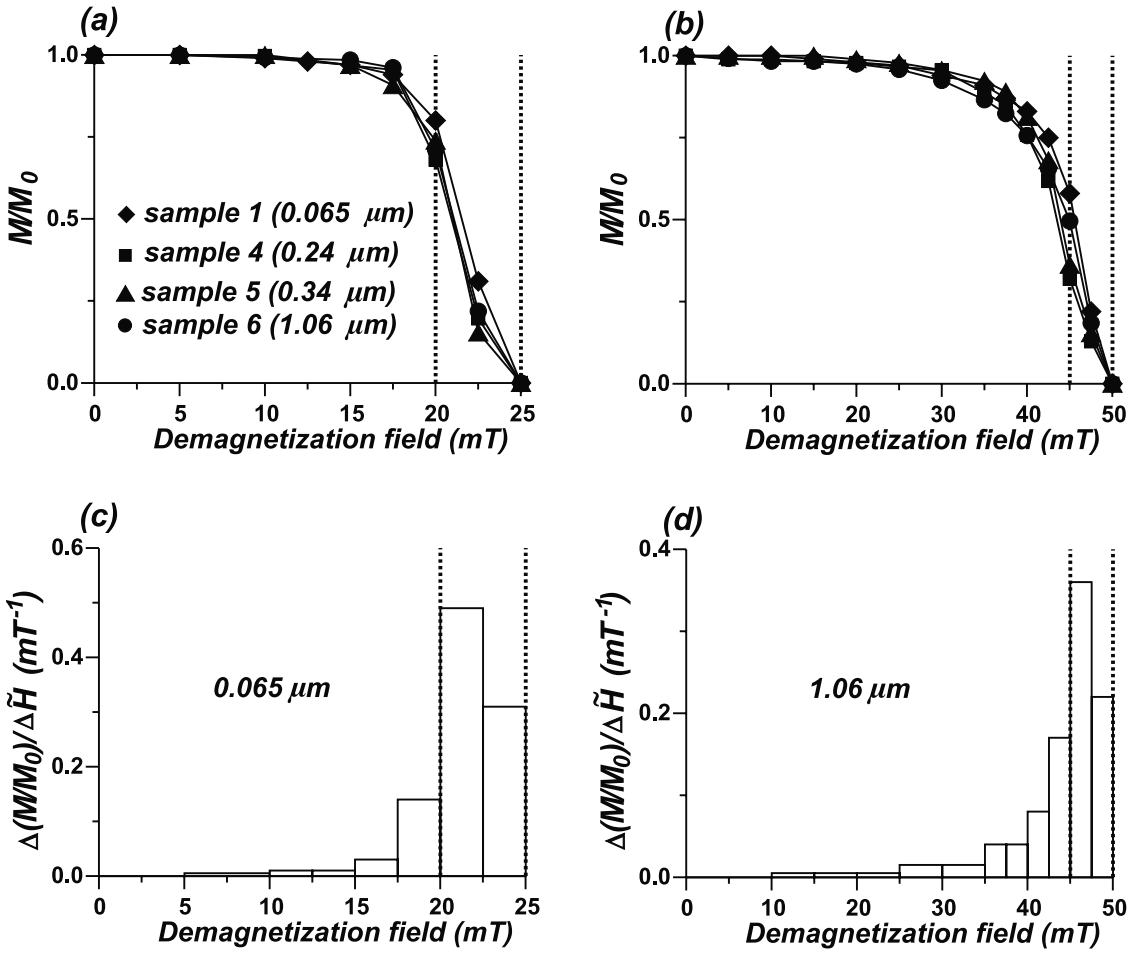

Figure 2. (a–b) Results of AF demagnetization of pARM^m (25 mT, 20 mT) and of pARM^n (50 mT, 45 mT) for synthetic SD and PSD magnetites. (c–d) Corresponding coercivity spectra of samples 1 and 6.

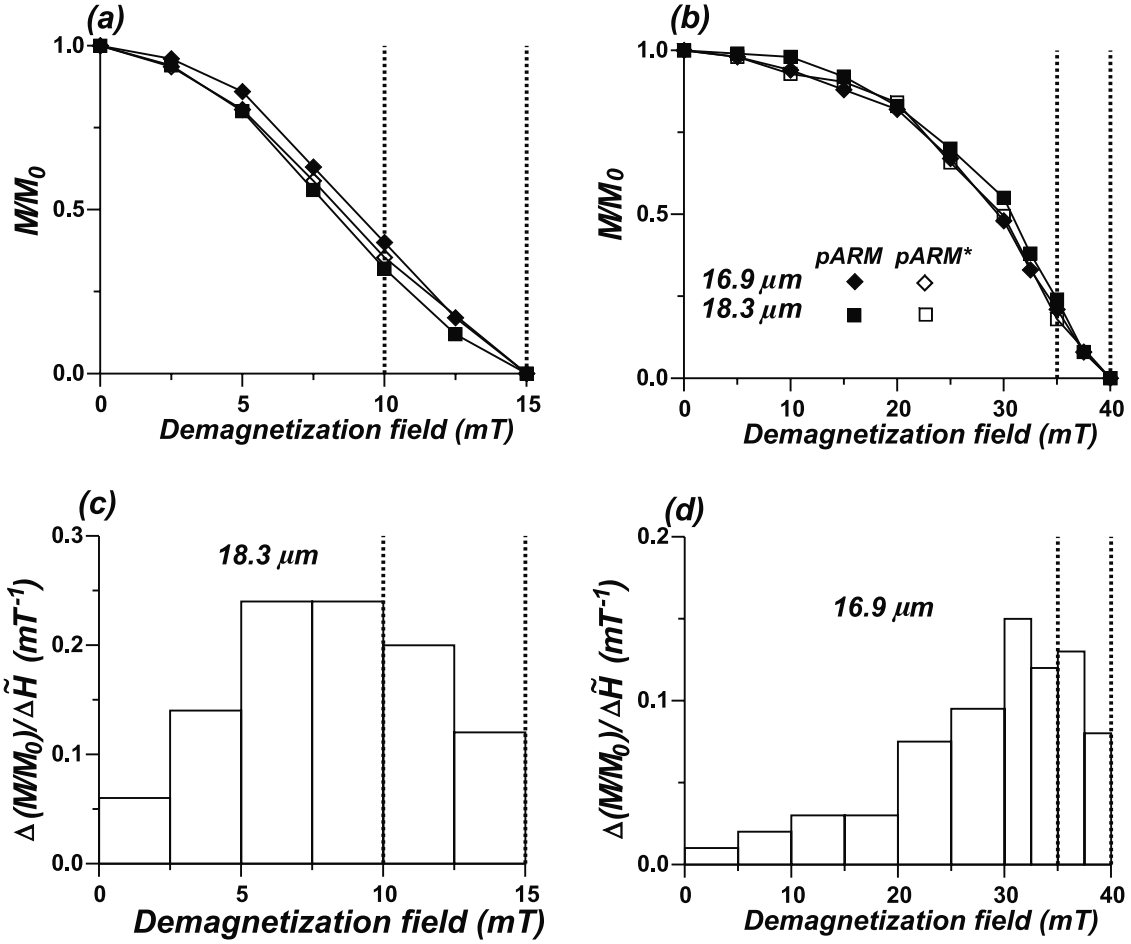

Figure 3. (a–b) Results of AF demagnetization of pARM^m (15 mT, 10 mT) and of pARM^n (40 mT, 35 mT) for synthetic MD magnetites. (c–d) Corresponding coercivity spectra for 16.9 μm and 18.3 μm.

demagnetized below the lower blocking field (10 or 35 mT). The coercivity spectra actually peak below the blocking range (Figures 3c and 3d).

3.2. Natural Samples

[8] Representative experimental data are shown in Figure 4 for natural samples 578 A (sediments from Lake Pepin, Minnesota [*Brachfeld and Banerjee*, 2000]), Km 3 (red scoria, Mount Aso, Japan [*Yu*, 1998]), and T 19 (Tudor Gabbro, Ontario [*Yu and Dunlop*, 2001]) (Figure 4). These samples have SD or PSD hysteresis properties (Table 3 and Figure 3 of paper 1). Although more of the pARM unblocked below the AF blocking range than in the synthetic SD and small PSD samples (Figure 2), the coercivity spectra peak within the blocking field interval (Figures 4c and 4d).

[9] Samples Bu 5 and 8 (Burchell Lake Granite, Ontario [*Dunlop*, 1984]) and S 50 (Shelley Lake Granite, Ontario [*Dunlop et al.*, 1984]) have MD hysteresis properties (Table 3 and Figure 3 of paper 1). Their pARM unblocking properties are also consistent with MD behavior. 70–90% of pARM^m and pARM^n unblocked below the blocking ranges of 15–20 and 20–25 mT (Figures 5a and 5b). The coercivity spectra have major low-coercivity tails and peak below the blocking field interval (Figures 5c and 5d).

4. Effect of Magnetic Prehistory on pARM

[10] Different initial states are known to affect the thermal demagnetization of pTRM and viscous remanent magnetization of MD and coarse PSD grains [*Vinogradov and Markov*, 1989; *Halgedahl*, 1993; *Shcherbakova et al.*, 2000; *Dunlop and Özdemir*, 2000, 2001]. We tested whether the same is true for the AF demagnetization of pARMs. We produced pARM^n* ($\widetilde{H}_d$, $\widetilde{H}_c$) in an AF decaying from 100 mT to $\widetilde{H}_d$ with zero added field, from $\widetilde{H}_d$ to $\widetilde{H}_c$ with an added steady field H, and from $\widetilde{H}_c$ to 0 with zero added field (Figure 6). The essential difference between the two remanences is that the upper field $\widetilde{H}_d$ of the pARM, at which H was switched on, was approached from below in the case of pARM^n but from above for pARM^n* (compare Figures 1 and 6).

[11] Intensities of pARM^n* and pARM^n for selected samples are listed in Table 1. Relative intensities are plotted in Figure 7. For SD and PSD samples 1 (0.065 μm), 4 (0.24 μm), 5 (0.34 μm), 6 (1.06 μm), 456 A, 578 A, T 19, and C 12 (Cordova Gabbro, Ontario [*Yu and Dunlop*, 2002]), the intensities of pARM^n* and pARM^n are almost identical.

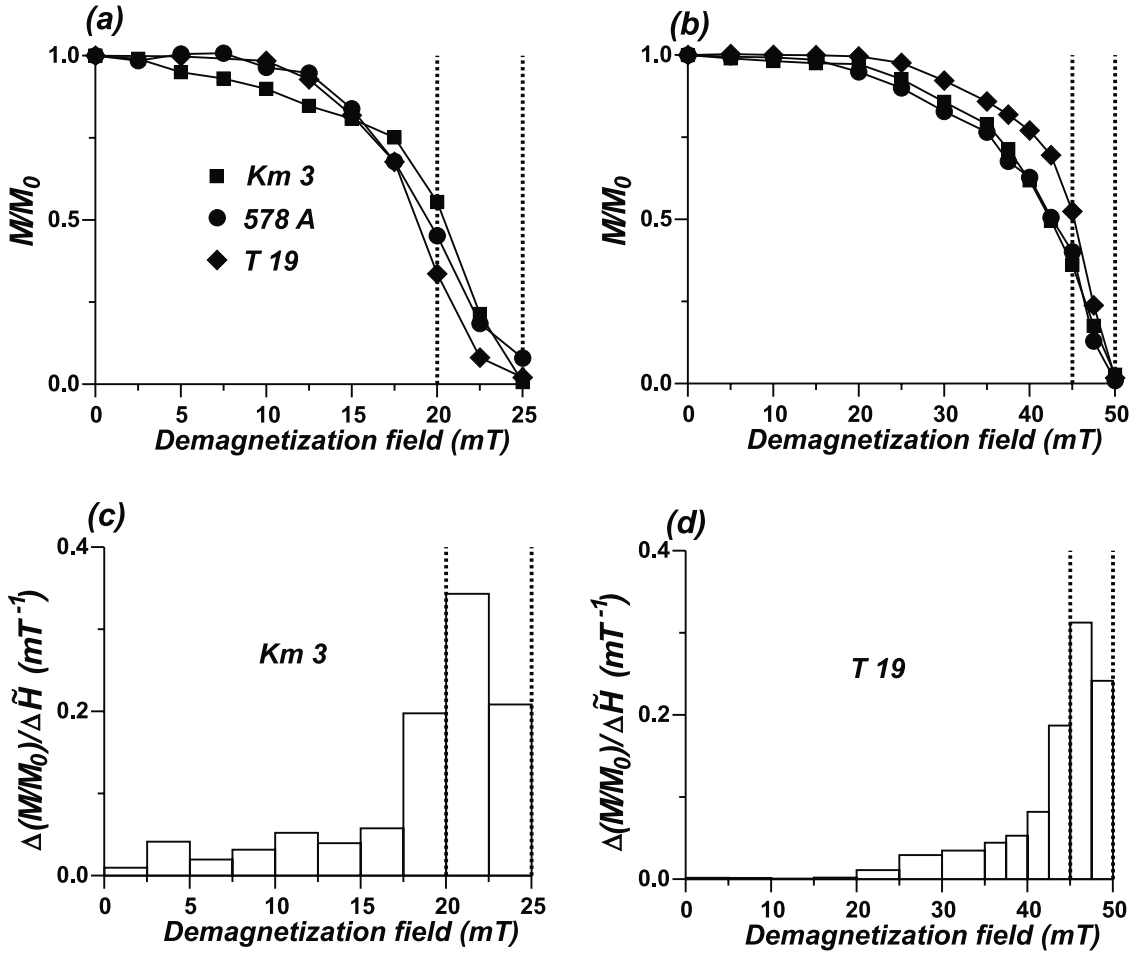

Figure 4. (a–b) The results of stepwise AF demagnetization of pARMs for sample 578 A (lake sediments, Lake Pepin, Minnesota [*Brachfeld and Banerjee*, 2000]), Km 3 (red scoria, Mount Aso, Japan [*Yu*, 1998]), and T 19 (Tudor Gabbro, Ontario [*Yu and Dunlop*, 2001]). (c–d) Corresponding coercivity spectra of Km 3 and T 19.

However, for large PSD and MD samples 9 (16.9 μm), 10 (18.3 μm), Bu 5, Bu 8, and S 50, $pARM^n$* is 6–14% more intense than $pARM^n$.

[12] A comparison of pARM* and pARM intensities in eight different field intervals covering the entire 0–40 mT coercivity range appears in Table 2. The pARM* > pARM in all field intervals but the difference is most accentuated for the lower fields. Despite this bias, the normalized AF demagnetization curves of pARM* and pARM are almost indistinguishable (Figure 3).

[13] In the case of MD pTRMs, it has been observed that a thermally cooled (TC) pTRM (heated to T_c and cooled to the upper blocking temperature in zero field, before switching on H: the analog of $pARM^n$*) has higher intensity than a thermally heated (TH) pTRM (thermally demagnetized and then heated to the upper blocking temperature in zero field, before applying H: the analog of $pARM^n$). Our results are consistent with this pattern. According to *Shcherbakova et al.* [2000], the difference between TC and TH pTRM intensities quantitatively matches the TC thermal demagnetization tail extending above the upper blocking temperature to the magnetite Curie point (TH pTRMs had only minor tails). We have not observed any high-coercivity tail in AF demagnetization of either $pARM^n$ or $pARM^n$*, implying a fundamental difference between pARM and pTRM phenomena, most likely different MD magnetic microstates or domain configurations.

5. Discussion

5.1. Reciprocity of pARMs

[14] The AF demagnetization behavior of narrow-band pARMs for synthetic samples is grain-size dependent (Figures 2 and 3). The pARMs of SD and small PSD size samples demagnetize mainly over the AF range in which pARM was originally blocked. They thus obey the pARM reciprocity law: blocking and unblocking are equivalent processes. On the other hand, pARMs of MD size grains demagnetize readily below the lower blocking field. Their coercivity spectra have large low-coercivity tails and actually peak below the lower pARM blocking field (Figure 3).

[15] The lake sediments and gabbros used in this study had intermediate AF behavior, with about 50% of pARM demagnetizing over the field blocking range (Figure 4). They nevertheless have previously yielded successful paleointensity results by the pseudo-Thellier and Thellier meth-

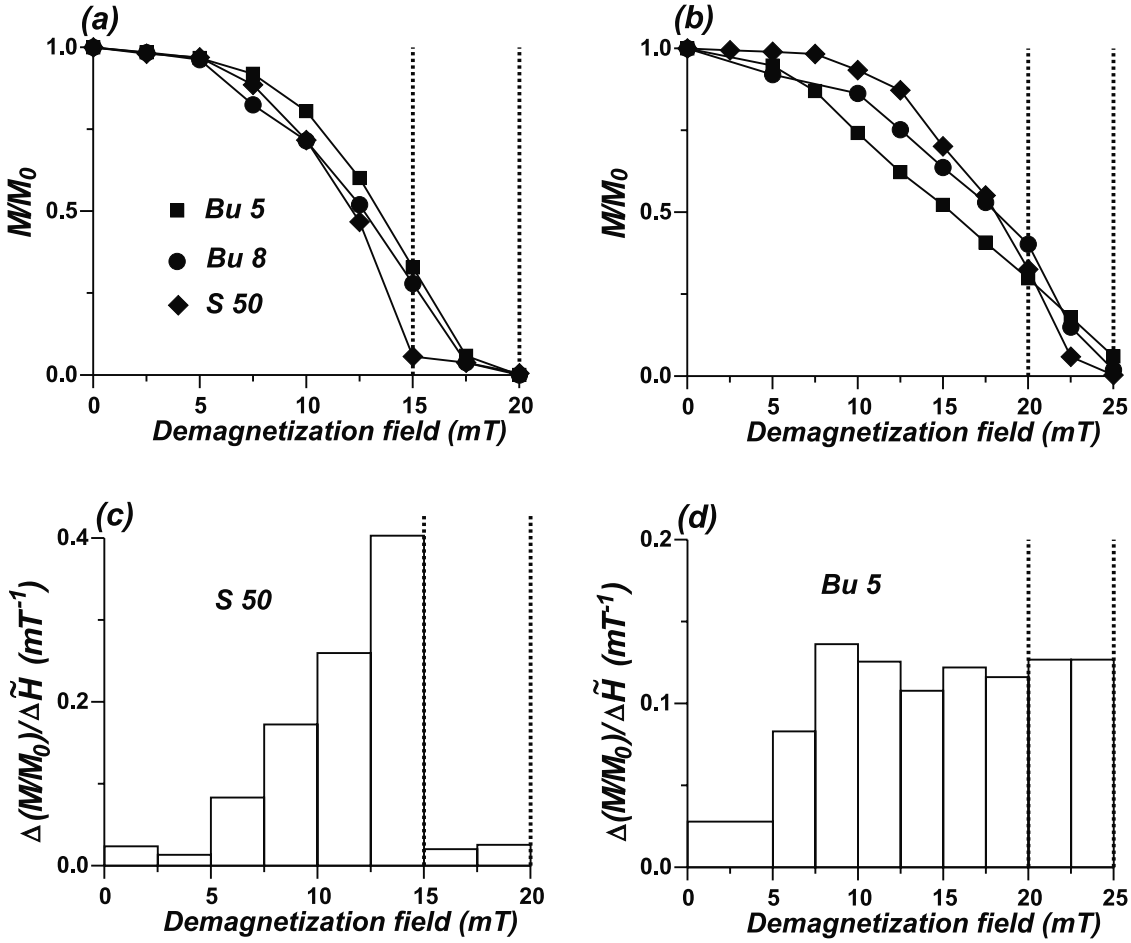

Figure 5. (a–b) The results of stepwise AF demagnetizations of Bu 5 and 8 (Burchell Lake Granite, Ontario [*Dunlop*, 1984]) and S 50 (Shelley Lake Granite, Ontario [*Dunlop et al.*, 1984]). (c–d) Corresponding coercivity spectra of S 50 and Bu 5.

ods, respectively [*Brachfeld and Banerjee*, 2000; *Yu and Dunlop*, 2001, 2002]. This success is rather surprising in view of their ambivalent behavior in pARM reciprocity experiments.

5.2. Implications for Paleointensity Determination

[16] It is interesting to compare the AF demagnetization of narrowband pARM to thermal demagnetization of narrowband pTRM. Whereas MD grains always have high-unblocking temperature tails [e.g., *Bolshakov and Shcherbakova*, 1979], MD and SD samples alike have no high-coercivity tails during AF demagnetization of pARM (Figures 2–5). The pARM ($\widetilde{H}_2$, $\widetilde{H}_1$) produced by a steady field H between $\widetilde{H}_2$ and $\widetilde{H}_1$ always demagnetizes totally in an AF of $\widetilde{H}_2$. The lack of a high-coercivity tail in pARM does not necessarily imply superiority of pARM methods of paleointensity determination, however. Low-temperature tails cause large thermal demagnetization of MD and PSD pTRM below the blocking temperature range and this in turn results in non-linear paleointensity behavior [*Dunlop and Özdemir*, 2000, 2001]. Low-coercivity pARM tails, which are prominent in our large PSD and MD samples (Figures 3 and 5) can be expected to have the same effect in pseudo-Thellier paleointensity experiments.

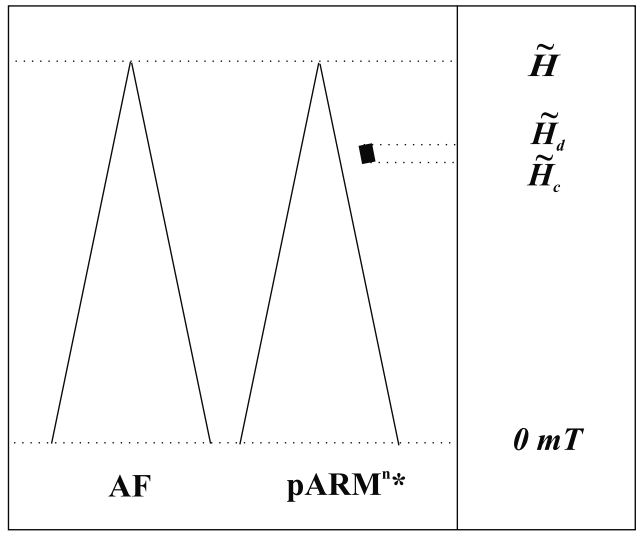

Figure 6. Schematic diagrams representing pARM^n* ($\widetilde{H}_d$, $\widetilde{H}_c$) acquisition: pARM^n* was produced starting from a peak AF of 100 mT, with the added steady field H on from $\widetilde{H}_d$ to $\widetilde{H}_c$.

Table 1. Comparison of Intensities Between $pARM^n$* and $pARM^n$

Sample	$pARM^n$*, mA/m	$pARM^n$, mA/m	$pARM^n$* − $pARM^n$, Difference, %
0.065 μm	1.16	1.14	1.75
0.24 μm	1.85	1.81	2.21
0.34 μm	0.90	0.91	−1.10
1.06 μm	1.19	1.19	0.18
16.9 μm	3.06	2.69	13.75
18.3 μm	5.60	5.20	7.69
456 A	11.65	11.61	0.34
578 A	15.72	15.51	1.35
T 19	132.19	130.24	1.50
C 12	18.66	18.14	2.87
Bu 5	28.00	25.55	9.59
Bu 8	16.16	15.23	6.11
S 50	64.39	58.68	9.40

[17] To test this anticipated effect, we performed simulated pseudo-Thellier paleointensity determinations [*Tauxe et al.*, 1995] on our synthetic samples. A total ARM (simulating natural remanent magnetization) was progressively AF demagnetized and its remanence loss partially replaced in pairs of companion steps at increasing AF levels. A plot of ARM remaining versus pARM gained, the analog of the Arai plot [*Nagata et al.*, 1963], shows an interesting grain-size dependence (Figure 8). Sample 1 (0.065 μm) comes closest to matching the ideal SD line. The MD sample (18.3 μm) has the largest deviations from this ideal line. Its strongly convex downward curve indicates that pARM lost in lower coercivity AF steps is larger than pARM gained in the same AF steps. For the PSD samples (0.24 and 1.06 μm), the downward curvature is less but still appreciable.

[18] Similar but more pronounced downward curvature has been observed in Arai plots for simulated Thellier experiments on PSD/MD magnetites [*Levi*, 1977; *Dunlop and Özdemir*, 1997, 2001]. In practical applications, the pseudo-Thellier method therefore offers certain advantages. The sagging of the pseudo-Arai plot is less severe and would lead to a smaller error if paleointensity was estimated by fitting a line to the first few data points. More importantly, only a tail in the coercivity distribution can cause convex-down curves in the pseudo-Thellier method, whereas corresponding curvature in Thellier heating results could well be caused by chemical alteration of the magnetic minerals rather than low- or high-temperature pTRM tails.

Table 2. Comparison of Intensities of pARM* and pARM for Synthetic MD Samples

$\widetilde{H}_B$,[a] mT	pARM*, mA/m	pARM, mA/m	$pARM^n$* − $pARM^n$ Difference, %
16.9 μm			
5–0	8.35	6.39	30.7
10–5	16.70	12.95	29.0
15–10	15.84	10.93	44.9
20–15	9.55	7.79	22.6
25–20	5.44	4.73	15.0
30–25	4.73	4.17	13.4
35–30	5.03	4.69	7.2
40–35	3.06	2.69	13.8
18.3 μm			
5–0	16.99	12.35	37.6
10–5	32.66	25.03	30.5
15–10	26.81	21.13	26.9
20–15	18.27	15.06	21.3
25–20	12.01	9.32	28.9
30–25	11.59	9.86	17.5
35–30	10.74	8.78	22.3
40–35	5.60	5.20	7.7

[a] $\widetilde{H}_B$ is the blocking field range.

6. Phenomenological Modeling

[19] Traditionally, magnetic properties of isothermal processes such as AF demagnetization or ARM acquisition have been analyzed using the Preisach diagram [*Preisach*, 1935; *Rimbert*, 1959; *Dunlop and West*, 1969]. Although Preisach diagrams provide both qualitative and quantitative information, their interpretation can be difficult or inconclusive [*Dunlop et al.*, 1990]. Instead we will adapt a recent phenomenological model used successfully to interpret pTRM behavior [*Fabian*, 2000, 2001] to analyze pARM reciprocity.

[20] Our phenomenological model of pARMs represents the magnetic behavior of a sample by a large number of independent loops, each defined by two coercivities or switching fields, for pARM blocking ($\widetilde{H}_B$) and unblocking

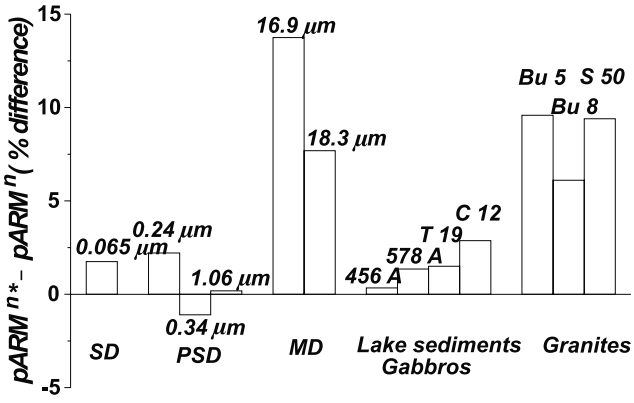

Figure 7. Percentage difference between $pARM^n$* ($\widetilde{H}_d$, $\widetilde{H}_c$) and $pARM^n$ ($\widetilde{H}_d$, $\widetilde{H}_c$).

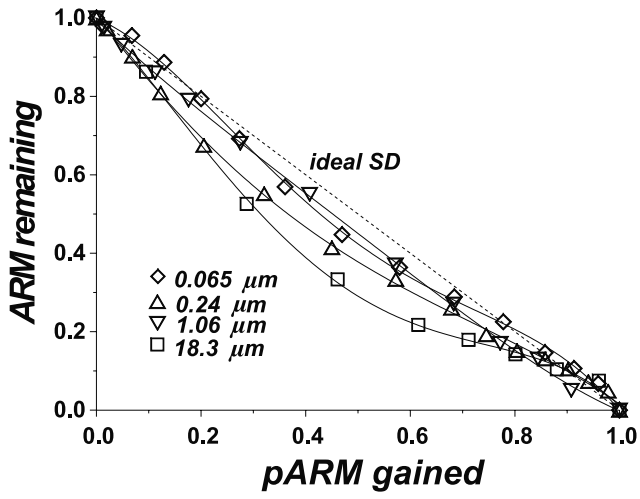

Figure 8. Results of pseudo-Thellier simulation experiments for some of the synthetic magnetites.

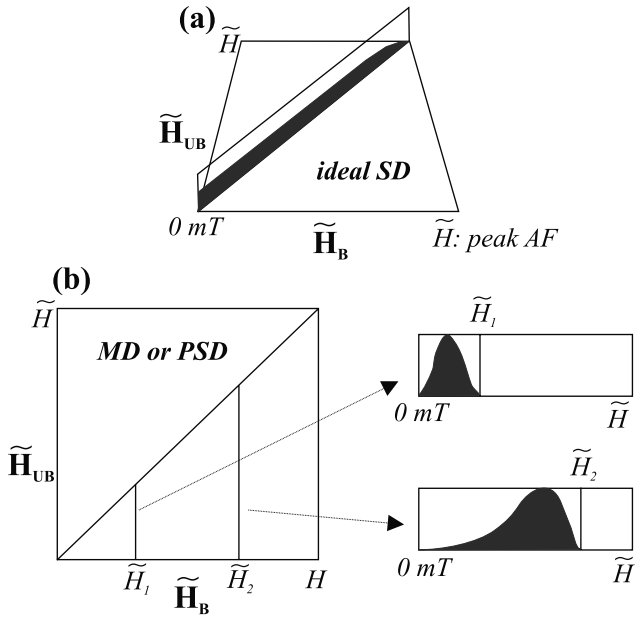

Figure 9. Schematic sketches of the distribution of $\widetilde{H}_{UB}$ versus $\widetilde{H}_B$. (a) Ideal SD grains have identical $\widetilde{H}_{UB}$ and $\widetilde{H}_B$. (b) For PSD and MD grains, $\widetilde{H}_{UB}$ is distributed up to but not beyond the diagonal line $\widetilde{H}_{UB} = \widetilde{H}_B$. The shaded areas depict possible $\widetilde{H}_{UB}$ distributions.

($\widetilde{H}_{UB}$). The number of loops in a particular area of the ($\widetilde{H}_{UB}$) vs. ($\widetilde{H}_B$) diagram is given by the density function, χ ($\widetilde{H}_B$, $\widetilde{H}_{UB}$). Two possible forms of χ are illustrated in Figure 9. For ideal SD grains, χ is confined to the diagonal, i.e., $\widetilde{H}_B = \widetilde{H}_{UB}$ (Figure 9a). PSD and MD grains have coercivity distributions extending up to but not beyond the AF at which steady field H is switched on in pARM acquisition (Figure 9b). A distinctive feature of pARM modeling compared to pTRM modeling [*Fabian*, 2000, Figure 1] is that the distribution of χ (represented as shaded region) has been truncated along the diagonal, where $\widetilde{H}_B$, $\widetilde{H}_{UB}$, since there is no high-coercivity pARM tail (Figures 2–5). In pTRMs, both low-temperature ($T_{UB} \leq T_B$) and high-temperature ($T_{UB} \geq T_B$) tails are observed, where T_B (T_{UB}) is the blocking (unblocking) temperature [*Dunlop and Özdemir*, 2001]. The distribution of ($\widetilde{H}_{UB}$) for the soft coercivity fraction, $pARM^m$, is approximately Gaussian, while the hard coercivity fraction, $pARM^n$, has a skewed ($\widetilde{H}_{UB}$) distribution (Figures 3 and 9b).

6.1. Three-Dimensional Mapping of χ^* and χ ($\widetilde{H}_B$, $\widetilde{H}_{UB}$)

[21] In order to construct a three-dimensional (3-D) map of χ ($\widetilde{H}_B$, $\widetilde{H}_{UB}$), experimental steps 1 and 2 (section 2) were carried out in successive stages, starting from low AFs. First, pARM (5 mT, 0 mT) was produced, and then double AF demagnetization was performed to 5 mT in 2.5 mT steps. Next, pARM (10 mT, 5 mT) was produced and AF demagnetized to 10 mT. Similar pARMs were generated, incrementing the upper and lower limits of $\widetilde{H}_B$ by 5 mT each time, and then AF demagnetized from 0 mT to the upper $\widetilde{H}_B$. No pARMs with $\widetilde{H}_B \geq 40$ mT were simulated because pARM (100 mT, 40 mT) is <2% of total ARM intensity for the MD samples. Constructing a 3-D map of χ^* ($\widetilde{H}_B$, $\widetilde{H}_{UB}$) was carried out using exactly the same experimental sequence as for χ, but with pARM*s rather than pARMs.

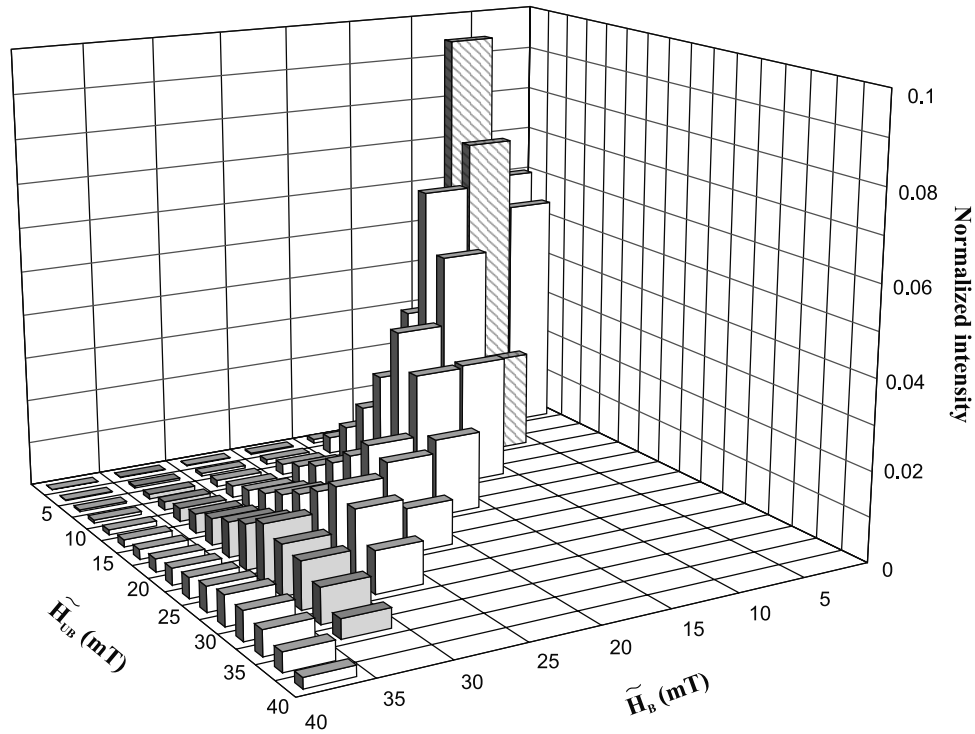

Figure 10. A three-dimensional view of the distribution χ ($\widetilde{H}_B$, $\widetilde{H}_{UB}$) for an MD sample (18.3 μm magnetite).

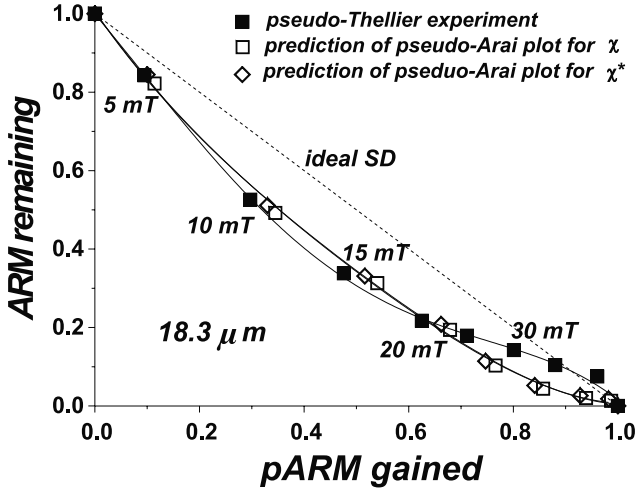

Figure 11. A comparison between the measured pseudo-Thellier results and the predicted pseudo-Arai plot for the 18.3 μm MD magnetite sample.

[22] The experimental spectrum χ ($\widetilde{H}_B$, $\widetilde{H}_{UB}$) for the 18.3 μm MD sample, normalized to total ARM intensity, is illustrated in Figure 10. The ($\widetilde{H}_B$, $\widetilde{H}_{UB}$) blocks are elongated because the increments of $\widetilde{H}_B$ were 5 mT but $\widetilde{H}_{UB}$ steps were 2.5 mT. Figure 10 demonstrates that for MD grains, the peak of χ for each $\widetilde{H}_{UB}$ lies well below the matching value of $\widetilde{H}_B$. The distribution χ^* ($\widetilde{H}_B$, $\widetilde{H}_{UB}$) is almost identical to χ ($\widetilde{H}_B$, $\widetilde{H}_{UB}$), except that the intensity of each block is higher.

6.2. Prediction of Pseudo-Arai Plots

[23] From the experimental spectra χ ($\widetilde{H}_B$, $\widetilde{H}_{UB}$), we made quantitative predictions of the results of pseudo-Thellier paleointensity simulations. We summed appropriate rows parallel to the H_B axis to find ARM lost at a particular H_{UB} level and we added columns parallel to the H_{UB} axis to find pARM or pARM* gained for a given value of H_B. The pseudo-Arai plots constructed in this way (Figure 11, open squares (diamonds) for $\chi(\chi^*)$) agree well with direct measurements (solid squares) for AF values below about 30 mT. The good agreement confirms that sagging of the pseudo-Arai plot is directly caused by low-coercivity ($\widetilde{H}_{UB} < \widetilde{H}_B$) fractions of pARMs. For AF values of 30 mT and above, the measured and predicted curves diverge. The direct measurements return to and even overshoot the ideal SD line, as one would expect if there were a high-coercivity tail of the pARM coercivity spectrum, whereas the χ ($\widetilde{H}_B$, $\widetilde{H}_{UB}$) predictions remain well below the ideal line. Since experimentally no high-coercivity tails were observed for any sample, this dichotomy is puzzling.

[24] Possibly, the dichotomy originates in the difference between experimental procedures followed in determining χ or χ^* and those used in the pseudo-Thellier experiment. The pARMs or pARM*s used in constructing χ or χ^* are incremental: each one is produced by applying H over a narrow AF range, e.g., 35–30 mT. The pARMs gained in the pseudo-Thellier experiment are cumulative: each is produced by applying H over a broad range of AF extending down to zero, e.g., 35–0 mT. Another difference is that AF demagnetization follows pARM production in the determination of χ or χ^*, whereas AF demagnetization precedes pARM acquisition in each pseudo-Thellier double step. These differences in process result in different initial states for χ or χ^* compared to pARM in the paleointensity experiment.

[25] Whatever its cause, the "rebound" of data points on the pseudo-Arai plot at higher AFs was observed for all pseudo-Thellier simulations, regardless of the grain size of magnetite (Figure 8). Evidently at higher coercivities, total ARM is more AF-resistant than partial ARMs produced in corresponding coercivity intervals. Possibly ARM favors metastable configurations such as metastable SD states, while domain walls develop in pARM acquisition at higher AF. To date, magnetic domain observations have been carried out for TRM and saturation remanence (SIRM) states but not for ARM. Metastable SD behavior has been observed for natural magnetite (10-20 μm, SIRM) [*Boyd et al.*, 1984], natural titanomagnetite (Ti content of 60%, TM60) >30 μm in size (TRM, H = 3 mT) [*Metcalf and Fuller*, 1988], and synthetic 25–50 μm TM60 (TRM, H = 42 μT) [*Halgedahl*, 1991].

[26] Similar rebound back to and past the ideal SD line on the Arai plot has been observed for high-temperature points in Thellier simulations [*Dunlop and Özdemir*, 2001; S. Xu and D. J. Dunlop, unpublished data, 1995] but is not predicted for synthetic Arai plots [*Fabian*, 2001] or in other theoretical predictions [*Dunlop and Özdemir*, 1997]. This phenomenon seems to be one of the missing links in our complete understanding of paleointensity determination.

6.3. Additivity of pARMs

[27] Another feature of our phenomenological model is that it accounts for the additivity of pARMs, as illustrated in Figure 12. The shaded areas represent the coercivity fractions that acquire pARMs between AF limits ($\widetilde{H}_2$, $\widetilde{H}_1$), ($\widetilde{H}_3$, $\widetilde{H}_2$) and ($\widetilde{H}_3$, $\widetilde{H}_1$). The first two areas sum to give the third area, whatever the details of the coercivity distribution. In other words, the density of points χ is immaterial to the validity of the pARM addition law.

[28] However, this picture is only partially valid in the case of MD magnetite, for which pARM < pARM* throughout the coercivity spectrum. By analogy with the law of additivity of partial TRMs, which is conventionally tested using pTRMs with a TC initial state, our experimental test of partial ARM additivity in paper 1 used pARM*s (Figure 6), not pARMs (Figure 1). As a result, the partial ARM additivity "law" in general is

$$\text{ARM} = \sum \text{pARM*} = \sum \text{pARM(SD and PSD, Table 1)}$$
$$\text{ARM} = \sum \text{pARM*} > \sum \text{pARM(MD, 1 and 2)}.$$

Although the partial ARMs in a pseudo-Thellier experiment are pARMs rather than pARM*s, the practical impact of

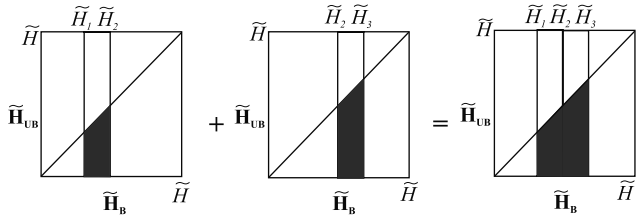

Figure 12. Graphical interpretation of the additivity of pARMs using the phenomenological model of Figure 9.

nonadditivity in the MD case is likely to be minimal because reliable paleointensities are invariably determined using SD or PSD magnetites.

7. Conclusions

1. Narrowband pARMs of SD and PSD grains were largely demagnetized over the same AF interval in which they were produced, i.e., unblocking field equals blocking field. In MD samples, coercivities were widely distributed below the blocking field range.

2. The low-coercivity tail of the pARM coercivity distribution of MD and large PSD grains causes nonlinear behavior in pseudo-Thellier paleointensity determination. The ARM loss always outweighs the pARM gained in matching AF steps, yielding a curved pseudo-Arai plot of ARM remaining versus pARM gained.

3. No high-coercivity tail has been observed during AF demagnetization of pARMs.

4. The intensity and AF demagnetization of pARM of MD grains depends on the initial state. However, pARM and pARM* have very similar normalized AF demagnetization curves.

5. The pseudo-Arai plot predicted from the experimentally determined distribution of unblocking versus blocking coercivities agreed well with the measured pseudo-Thellier simulation results, in particular providing a quantitative explanation for the convex-down form of the pseudo-Arai plots of MD samples.

6. The same model and distribution of blocking and unblocking fields explain the universal validity of the law of additivity of pARMs, observed in paper 1.

[29] **Acknowledgments.** We thank Stefanie Brachfeld and Jeff Gee for donating extensive collections of lake sediments and oceanic basalts. Mike Jackson, Lisa Tauxe, and Jean-Pierre Valet provided helpful reviews and suggestions. This research has been supported by the Natural Sciences and Engineering Research Council of Canada through grant A7709 to D.J.D.

References

Bolshakov, A. S., and V. V. Shcherbakova, A thermomagnetic criterion for determining the domain structure of ferromagnetics, *Izv. Phys. Solid Earth*, *15*, 111–117, 1979.

Boyd, J. R., M. Fuller, and S. L. Halgedahl, Domain wall nucleation as a controlling factor in the behavior of fine magnetic particles in rocks, *Geophys. Res. Lett.*, *11*, 193–196, 1984.

Brachfeld, S. A., and S. K. Banerjee, A new high-resolution geomagnetic relative paleointensity record for the North American Holocene: A comparison of sedimentary and absolute intensity data, *J. Geophys. Res.*, *105*, 821–834, 2000.

Dunlop, D. J., Paleomagnetism of Archean rocks from northwestern Ontario, 4, Burchell Lake granite, Wawa-Shebandowan Subprovince, *Can. J. Earth Sci.*, *21*, 1098–1104, 1984.

Dunlop, D. J., and Ö. Özdemir, *Rock Magnetism: Fundamentals and Frontiers*, 573 pp., Cambridge Univ. Press, New York, 1997.

Dunlop, D. J., and Ö. Özdemir, Effect of grain size and domain state on thermal demagnetization tails, *Geophys. Res. Lett.*, *27*, 1311–1314, 2000.

Dunlop, D. J., and Ö. Özdemir, Beyond Néel's theories: Thermal demagnetization of narrow-band partial thermoremanent magnetization, *Phys. Earth Planet. Inter.*, *126*, 43–57, 2001.

Dunlop, D. J., and G. F. West, An experimental evaluation of single domain theories, *Rev. Geophys.*, *7*, 709–757, 1969.

Dunlop, D. J., L. D. Schutts, and C. J. Hale, Paleomagnetism of Archean rocks from northwestern Ontario, 3, Rock magnetism of the Shelley Lake granite, Quetico Subprovince, *Can. J. Earth Sci.*, *21*, 879–886, 1984.

Dunlop, D. J., M. F. Westcott-Lewis, and M. E. Bailey, Preisach diagrams and anhysteresis: Do they measure interactions?, *Phys. Earth Planet. Inter.*, *65*, 62–77, 1990.

Fabian, K., Acquisition of thermoremanent magnetization in weak magnetic fields, *Geophys. J. Int.*, *142*, 478–486, 2000.

Fabian, K., A theoretical treatment of paleointensity determination experiments on rocks containing pseudo-single or multidomain magnetic particles, *Earth. Planet Sci. Lett.*, *188*, 45–58, 2001.

Halgedahl, S. L., Magnetic domain patterns observed on synthetic Ti-rich titanomagnetite as a function of temperature and in states of thermoremanent magnetization, *J. Geophys. Res.*, *96*, 3943–3972, 1991.

Halgedahl, S. L., Experiments to investigate the origin of anomalously elevated unblocking temperatures, *J. Geophys. Res.*, *98*, 22,443–22,460, 1993.

Levi, S., The effect of magnetite particle size on paleointensity determinations of the geomagnetic field, *Phys. Earth Planet. Inter.*, *13*, 245–259, 1977.

Metcalf, M., and M. Fuller, A synthetic TRM induction curve for fine particles generated from domain observations, *Geophys. Res. Lett.*, *15*, 503–506, 1988.

Nagata, T., Y. Arai, and K. Momose, Secular variation of the geomagnetic total force during the last 5000 years, *J. Geophys. Res.*, *68*, 5277–5281, 1963.

Preisach, F., Uber die magnetische Nachwirkung, *Z. Phys.*, *94*, 277–302, 1935.

Rimbert, F., Contribution à l'étude de l'action de champs alternatifs sur les aimantations rémanentes des roches, Applications géophysiques, *Rev. Ins. Fr. Pét.*, *14*, 17–54, 123–155, 1959.

Shcherbakova, V. V., V. P. Shcherbakov, and F. Heider, Properties of partial thermoremanent magnetization in pseudo-single-domain and multidomain magnetite grains, *J. Geophys. Res.*, *105*, 767–781, 2000.

Tauxe, L., T. Pick, and Y. S. Kok, Relative paleointensity in sediments: A pseudo-Thellier approach, *Geophys. Res. Lett.*, *22*, 2885–2888, 1995.

Thellier, E., Sur l'aimantation des terres cuites et ses applications géophysiques, *Ann. Inst. Phys. Globe Univ. Paris Bur.*, *16*, 157–302, 1938.

Thellier, E., and O. Thellier, Sur l'intensité du champ magnétique terrestre dans le passé historique et géologique, *Ann. Geophys.*, *15*, 285–376, 1959.

Vinogradov, Y. K., and G. P. Markov, On the effect of low temperature heating on the magnetic state of multidomain magnetite, in *Investigations in Rock Magnetism and Paleomagnetism* (in Russian), pp. 31–39, Inst. of Phys. of the Earth, Moscow, 1989.

Yu, Y., Rock magnetic and paleomagnetic experiments on hemoilmenites and titanomagnetites in some volcanic rocks from Japan, M. Sc thesis, 24 pp., Univ. of Toronto, Toronto, Ont., 1998.

Yu, Y., and D. J. Dunlop, Paleointensity determination on the Tudor Gabbro, southern Ontario, *J. Geophys. Res.*, *106*, 26,331–26,343, 2001.

Yu, Y., and D. J. Dunlop, Multivectorial paleointensity determination from the Cordova Gabbro, southern Ontario, *Earth Planet. Sci. Lett.*, in press, 2002.

Yu, Y., D. J. Dunlop, and Ö. Özdemir, Partial anhysteretic remanent magnetization in magnetite, 1, Additivity, *J. Geophys. Res.*, *107*, doi:10.1029/2001JB001249, in press, 2002.

D. J. Dunlop, Ö. Özdemir, and Y. Yu, Room 3004, South Building, Geophysics, Department of Physics, University of Toronto at Mississauga, 3359 Mississauga Road North, Mississauga, Ontario, Canada L5L 1C6. (dunlop@physics.utoronto.ca; ozdemir@physics.utoronto.ca; yjyu@physics.utoronto.ca)